Adipose-tissue derived signals control bone remodelling.

He Fu[1], Maria-Bernadette Madel[2,3], Dominique D. Pierroz[4], Mariano Schiffrin[1], Carine Winkler[1], Anne Wilson[5], Cécile Pochon[6], Barbara Toffoli[1], Jean-Yves Jouzeau[6], Federica Gilardi[1], Serge Ferrari[7], Nicolas Bonnet[7], Claudine Blin-Wakkach[2,3], Béatrice Desvergne[1*] and David Moulin[6*]

[1]Center for Integrative Genomics, Genopode, Lausanne Faculty of Biology and Medicine CH-1015 Lausanne, Switzerland; [2] CNRS UMR7370, Laboratoire de PhysioMédecine Moléculaire, Nice, France; [3]Université Côte d'Azur, Nice, France; [4]International Osteoporosis Foundation, 1260 Nyon, Switzerland; [5]Ludwig Centre for Cancer Research, Department of Oncology, University of Lausanne, 1066 Epalinges, Switzerland, [6]IMoPA, Biology and Health, UMR-7365 CNRS, University of Lorraine, France ; and [7]Division of Bone Diseases, Department of Internal Medicine Specialties, Geneva University Hospital & Faculty of Medicine, Geneva 14, Switzerland

*These authors contributed equally and are corresponding authors.

Summary

Long bones from mammals' host blood cell formation and contain many multiple cell types, including adipocytes. Excessive presence of adipocytes in bone marrow is associated with pathological conditions such as age-related osteoporosis or marrow aplasia induced by irradiation or chemotherapy. However, physiological functions of bone marrow adipocytes are poorly documented. Here, we investigated the consequence of total adipocyte deficiency on bone homeostasis in mice. By generating adipocyte-deficient mice using PPARγ deletion, we found that lipoatrophy leads to dramatic alterations of trabecular and cortical femoral bone. Cortical bone is extremely porous and poorly defined due to the excessive presence of active bone-resorbing osteoclasts. Hence, our observation demonstrates that osteoclast formation occurs in the absence of PPARγ despite its supposed role in osteoclastogenesis. We found that two independent models of lipoatrophy recapitulated this phenotype, demonstrating that hyperosteoclastogenesis is not linked to intrinsic PPARγ deficiency. We further showed that adiponectin, a cytokine produced by adipocytes and mesenchymal stromal cells, is a potent inhibitor of osteoclastogenesis *in vitro* and *in vivo*. Furthermore, pharmacological activation of adiponectin receptors by the synthetic agonist AdipoRon is able to block mature osteoclast activity both in mouse and human by blocking podosome formation. Mechanistically, we demonstrated involvement of AMPK activation in the adiponectin-inhibiting action on mature osteoclasts, thereby demonstrating that even fully differentiated and active, osteoclasts are sensitive to adipose-derived signals. Lastly, we showed that AdipoRon inhibits bone erosion in vivo in a murine model of inflammatory bone loss. Collectively, these data reveal that adiponectin-producing cells are key regulators of bone homeostasis, and that preserving functional bone marrow adiponectin pathway can improve bone integrity in the context of metabolic and inflammatory disorders.

Keywords: Adiponectin, Osteoclast, Bone Marrow Adiposity, Cortical Bone porosity

Introduction

Physiological function of bone marrow resident adipocytes (BM-adipocyte) is scarcely understood (Horowitz et al., 2017). Beside calorie storage during fed conditions and energy release during fasting, adipocyte (including BM-adipocyte) also exert metabolic function at distance by secreting adipokines. The interest for adipokines in the context of bone homeostasis has been recently reinforced, after single cell global transcriptome analysis of bone cells, revealed that bone-forming (osteoblastic lineage) and bone resorbing cells (osteoclastic lineage) express adipokine receptors (notably and respectively leptin receptor and adiponectin receptor) in a specific pattern (Baryawno et al., 2019).

Peroxisome proliferator-activated receptors (PPARs) are ligand-activated transcription factors that belong to the nuclear hormone receptor superfamily. PPARγ is expressed during the differentiation of preadipocytes into adipocytes in white and brown adipose tissues (Tontonoz and Spiegelman, 2008), and represents a master regulator of adipogenesis. Indeed, loss-of-function studies both *in vitro* and *in vivo* have clearly demonstrated that PPARγ is essential for the formation of adipose tissue (Barak et al., 1999; Rosen et al., 1999; Wang et al., 2013a) and mature adipocyte homeostasis (Imai et al., 2004). This was further confirmed by the total lack of adipocytes in mice carrying a full body deletion of PPARγ ($\gamma^{\Delta/\Delta}$). Unlike in adipocytes, the role of PPARγ in osteoclasts, is far less understood, and has been a matter of controversy during the last decades (Wan et al., 2007; Zou et al., 2016).

Global and lipid metabolism 'sensing' of mature osteoclast, i.e. the fact that osteoclasts express functional nuclear and membrane receptors that are sensitive to adipose derived signals raises the question of a "dialog" between adipose tissues and these bone remodelling cells.

Therefore, genetically-induced lipoatrophic mice, (i.e. totally deficient in adipocytes) have been used in the present study to analyse the consequences of adipocyte and adipocyte-derived mediators' depletion on bone homeostasis and more specifically on osteoclasts.

Results

In order to test for an impact of adipose tissue on bone homeostasis, we generated lipoatrophic mice (through epiblastic (Sox2 promoter) *cre* deletion of the Pparg allele). These mice displayed dramatic alterations of both trabecular and cortical bones. Three-dimensional images generated by trabecular bone microcomputed tomography (3D micro-CT) reconstruction of the femurs of one-year old male and female mice highlighted a remarkable trabecularization of the bone architecture in $\gamma^{\Delta/\Delta}$ mice, which extends along the shaft and almost reaches the mid-diaphysis (VIDEO 1 , Fig. 1a). Interestingly, cortical bone was found to be extremely porous at the epiphysis and the diaphysis. It has to be noted that, owing to hypertrabecularization and high cortical porosity, the cortical bone is poorly defined in these mice.

Video of 3D micro-CT reconstruction of genetically induced lipoatrophic mice showing alterations of both trabecular and cortical femoral bone.

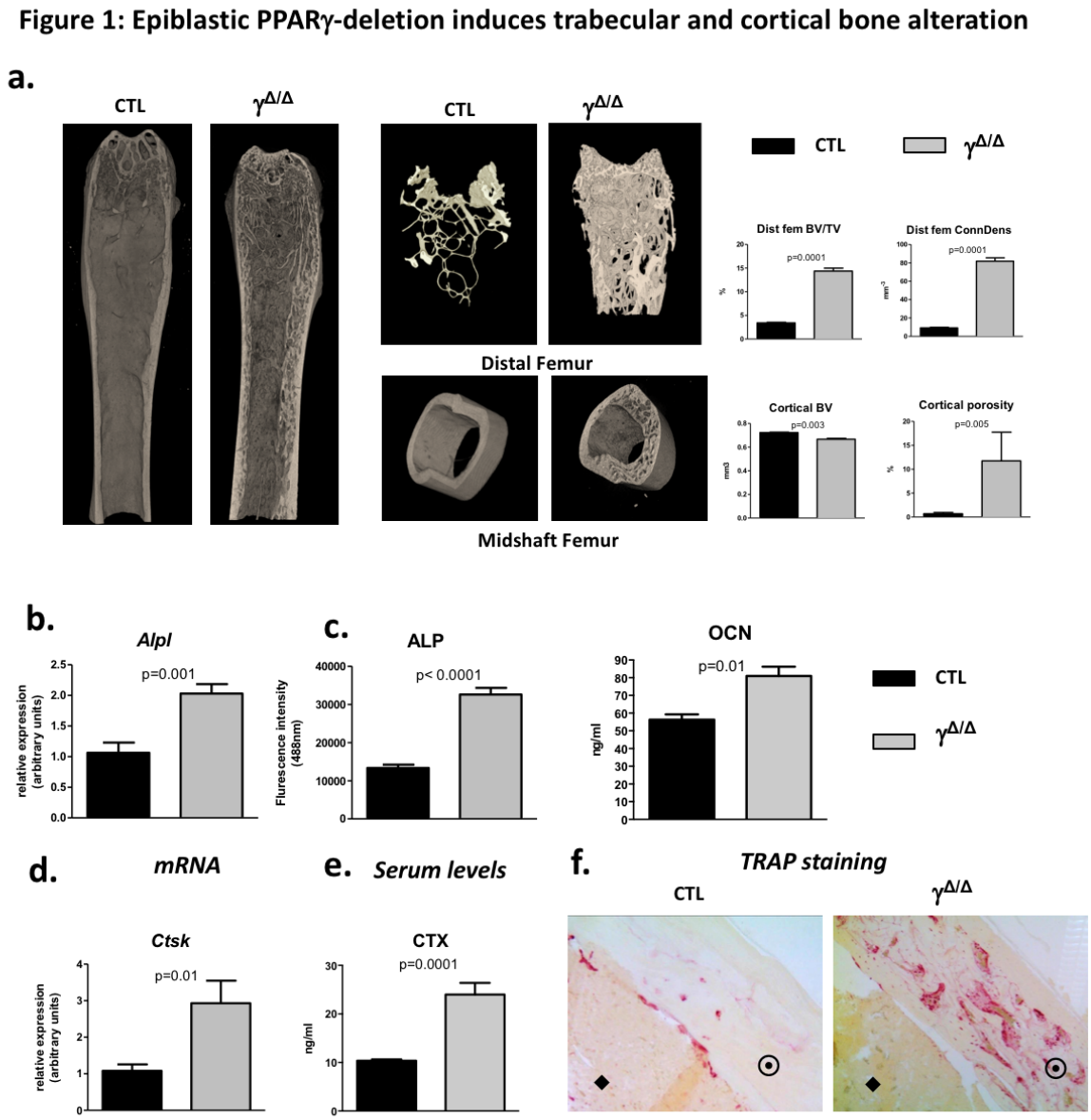

Figure 1: Epiblastic PPARγ-deletion induces trabecular and cortical bone alteration
a. Micro-CT analysis of femur from Ppar*g*$^{\Delta/\Delta}$ ($\gamma^{\Delta/\Delta}$) mice or control littermates (CTL). Histograms on the right show for the different genotypes (black bars for CTL and grey bars for $\gamma^{\Delta/\Delta}$) the percentage bone volume/trabecular volume (BV/TV) in % and connectivity density (ConnDens) of distal femoral trabecular bone (upper panels), and the cortical bone volume (BV) in mm^3 and the percentage of cortical porosity of femur (lower panels); n = 5 WT and 5 $\gamma^{\Delta/\Delta}$. All mice were 1-year-old. **b**. RT-qPCR analysis of Alkaline phosphatase (*AlpI*) gene expression in femur from CTL and $\gamma^{\Delta/\Delta}$; n = 6 WT and 7 $\gamma^{\Delta/\Delta}$. **c.** ELISA measurements of serum Alkaline phosphatase (ALP) and osteocalcin (OCN); n = 8 CTL and 8 $\gamma^{\Delta/\Delta}$. **d.** RT-qPCR analysis of cathepsin K (Ctsk) expression in femur from CTL and $\gamma^{\Delta/\Delta}$; n = 7 CTL and 7 $\gamma^{\Delta/\Delta}$. **e.** ELISA measurements of serum Carboxy-terminal Collagen I telopeptide (CTX); n= 8 CTL and 8 $\gamma^{\Delta/\Delta}$. **f.** Representative images of TRAcP staining of decalcified sections of femurs, at mid-shaft levels, from control (CTL) or *Pparg*$^{\Delta/\Delta}$ ($\gamma^{\Delta/\Delta}$) mice. ⊙ = cortical bone; ◆ = bone marrow. Data are presented as mean ± S.E.M. Statistical significance was determined by two-tailed unpaired *t*-test.

Molecular analyses confirmed an increased trabecular bone formation, as exemplified by alkaline phosphatase and osteocalcin increase measured by RT-qPCR and ELISA (Fig.1b and c). Three-D micro-CT of the fourth lumbar vertebrae clearly demonstrated increased trabecular bone volume fraction and trabecular connectivity density, indicating increased osteoblastogenesis in $\gamma^{\Delta/\Delta}$ as observed in (Akune et al., 2004) (and in Supplemental Data Fig. 1). These results are consistent with the pivotal role of PPARγ on the fate of bone marrow mesenchymal stromal cells, with previous reports showing increased osteoblastogenesis when PPARγ signalling is pharmacologically or genetically blocked (Takada et al., 2009). Remarkably, increased expression of bone resorbing markers such as cathepsin K (Fig. 1d) and carboxy-terminal collagen I telopeptide (Fig. 1e), were measured by RT-qPCR and ELISA, respectively, suggesting a parallel increase in osteoclastogenesis. TRAcP staining on femoral sections (Fig. 1f) confirmed the increased presence of bone-resorbing osteoclasts in cortical bone, explaining the observed cortical porosity.

PPARγ is known to play a role in osteoclastogenesis. More specifically, Tie2^{Cre}-directed deletion of PPARγ severely impaired osteoclastogenesis, whereas PPARγ synthetic agonists exacerbated it (Wan et al., 2007). This role of PPARγ in osteoclast have been recently questioned by the study of Zou *et al.*, showing that PPAR-γ regulates pharmacological but not physiological or pathological osteoclast formation (Zou et al., 2016). This raised the question whether the elevated osteoclast (OCL) activity observed in cortical bone is attributable to lipoatrophy, or to unforeseen intrinsic effects of PPARγ deficiency in the osteoclast lineage. In support of the lipoatrophy hypothesis, increased cortical porosity was also observed in the AZIP transgenic mouse, a lipoatrophic mouse with functional PPARγ signalling. In addition, we generated lipoatrophic mice with wild-type hematopoietic lineage by invalidating PPARγ in adipose tissue (Adipoq^{cre} PPARγ fl/fl, γ^{FatKO} (Wang et al., 2013b)). TRAcP staining of cortical bone and micro-CT analysis in these mice revealed increased osteoclast numbers and activity with an enhanced cortical porosity, as observed in $\gamma^{\Delta/\Delta}$ (Fig. 2a-c and Supplemental Data Fig. 2a-c). These two independent mouse models confirmed that adipocyte deficiency is pivotal to the cortical bone phenotype observed here.

To investigate how adipocytes regulate osteoclastogenesis, and to evaluate whether factors produced by adipocytes within the bone marrow can influence osteoclastogenesis, we performed an osteoclastogenesis assay using bone marrow cells from wild-type mice cultured in the presence of either control medium or adipocyte-conditioned medium (ACM). ACM was isolated from culture of adipocyte-differentiated 3T3-L1 cells whereas control medium (CTL)

was obtained from culture of undifferentiated pre-adipocytes 3T3-L1 cells (Fig. 2d). We observed a substantial decrease in the number of mature osteoclasts in the presence of ACM compared to preadipocyte-conditioned medium. Consistently, adipocyte-conditioned medium significantly inhibited bone resorption as assessed by calvaria resorption assay (Fig. 2ef). These data suggest that adipocyte-secreted mediators are responsible for the inhibition of RANKL-induced osteoclast differentiation *in vitro*.

Next, we searched for component(s) of ACM responsible for this anti-osteoclastogenic activity. Therefore, we filtered all components larger than 35 kDa from the conditioned medium and showed that the inhibitory activity was maintained despite the filtering. The molecular weights of the major adipokines, adiponectin and leptin, are below 35 kDa and their circulating levels are not or barely detectable in *Pparg*$^{\Delta/\Delta}$ mice ((Gilardi et al., 2019) and Supplemental Data Fig. 2d). Unlike *Leptin*, *Adiponectin* is preferently expressed by adipocyte and by bone-marrow MSC, and is a well-characterized target gene of PPARγ (Iwaki et al., 2003). Western-blot analyses confirmed that adiponectin was present in large amounts in ACM but not in CTL medium (Supplemental Data Fig. 2d). We therefore tested whether blocking adiponectin would affect ACM-mediated inhibition of osteoclastogenesis *in vitro*. As shown in Figure 2f, the addition of a blocking adiponectin antibody reversed the reduction in osteoclast number in a dose-dependent manner. These results suggest that the solubles factors secreted by adipocytes, in particular adiponectin, are inhibitors of osteoclastogenesis. We conclude that lipoatrophy, including in the bone marrow, results in a complete absence of this adipokine, leading to the loss of its repressive activity in osteoclast differentiation.

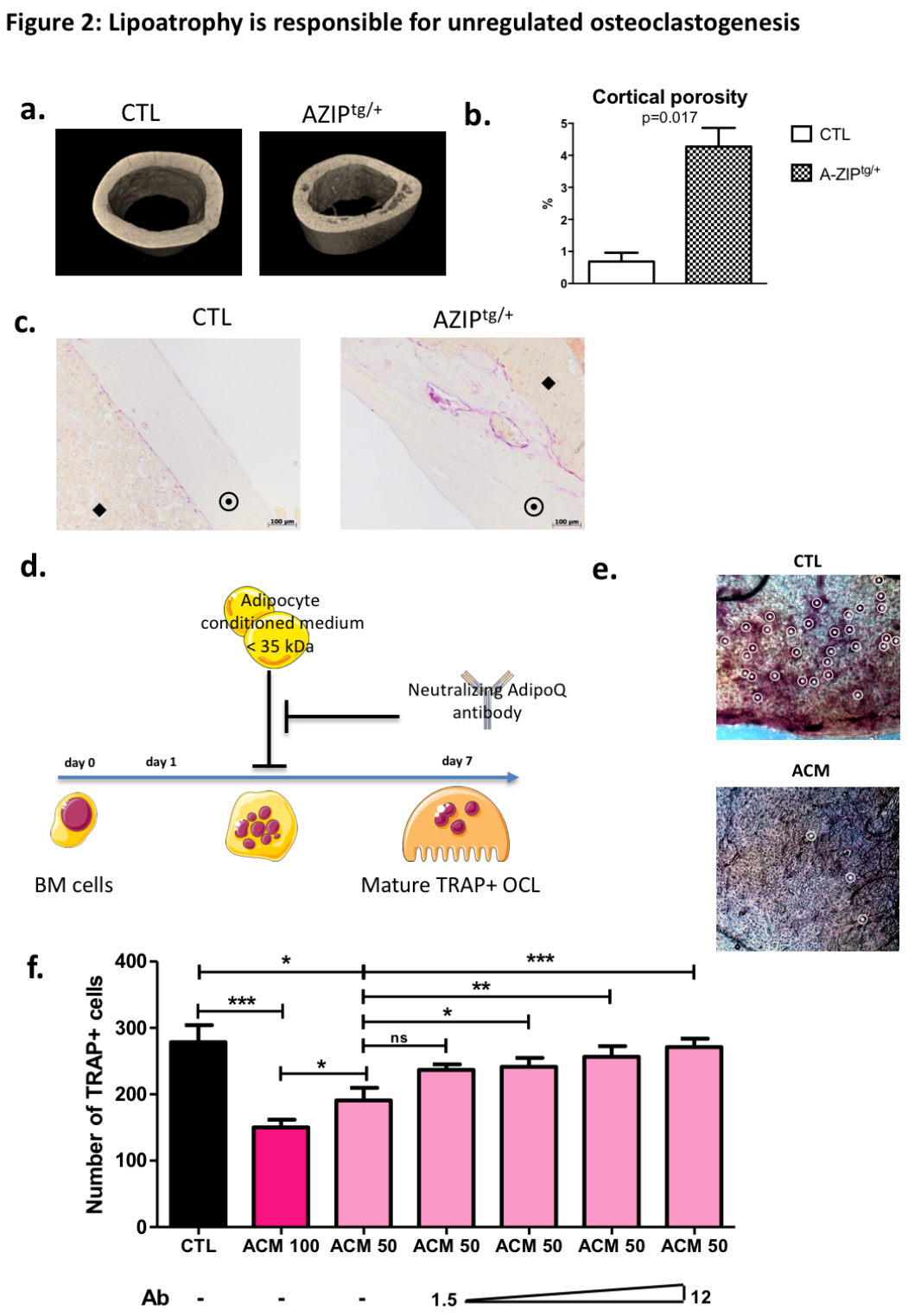

Figure 2: Lipoatrophy is responsible for unregulated osteoclastogenesis

a. . Representative 3D sections of midshaft femur from A-ZIP$^{tg/+}$ (n=6) and CTL (n=6) littermates. **b.** Femoral cortical porosity measured by micro-CT analysis of femur from A-ZIP$^{tg/+}$ (n=6) and control (CTL; n=6) littermates. **c.** Representative images of TRAcP staining of longitudinal sections of decalcified femurs, at mid-shaft levels, from control (CTL) or A-ZIP$^{tg/+}$ mice. ⊙ = cortical bone; ◆ = bone marrow. **d.** Experimental in vitro assay

used to test anti-osteoclastogenic activity from adipocyte secretome. **e**. Calvaria resorption pit assay. Representative sections of skulls from 14-day-old wild-type pups cultured for 2 weeks in complete aMEM in the presence of conditioned medium from either undifferentiated 3T3-L1 preadipocytes (CTL, n=3) or mature 3T3-L1 adipocytes (ACM, n=3). Data are presented as mean ± s.e.m. **f**. One day after plating, wild type BM cells were cultured for 6 more days in the presence of M-CSF and RANKL (osteoclast differentiation media) in addition to conditioned medium prepared from differentiated (ACM: adipocyte-conditioned medium) or undifferentiated (CTL: control-conditioned medium) 3T3-L1 preadipocytes. Different doses of a specific blocking antibody against adiponectin (1.5–12.0 μg/ml) were added to the conditioned medium (ACM50) during osteoclast differentiation (ACM 100 means pure ACM; ACM50 means 1:1 diluted ACM with osteoclast differentiation medium).

AdipoRon, a non-peptidic agonist of adiponectin receptors (Okada-Iwabu et al., 2013), recapitulated the blocking effect of ACM on osteoclast differentiation irrespective of the origin of the osteoclast progenitors (bone marrow, spleen, or macrophage-enriched fraction) with IC50 in the micromolar range (Fig. 3a, b Suplementary Fig. 3). Furthermore, AdipoRon is able to block osteoclast differentiation in Pparg deficient cells, confirming that intrinsic alterations do not play a role in the observed phenotype (Fig. 3c).

Previous studies demonstrated *in vivo* that mice treated with adiponectin expressing adenovirus have reduced osteoclast number and bone-resorption marker (Oshima et al., 2005) and adiponectin blocked *in vitro* osteoclastogenesis of RAW264 by inhibiting NFATc1. Blockade of NFATc1 was suggested to occur through activation of the AMPK signaling pathway, a key integrator of metabolic signals and target of adiponectin signalling, (Yamaguchi et al., 2008). Furthermore, Tu and colleagues demonstrated that the adaptor protein of adiponectin signalling, APPL1 mediates adiponectin signaling and reduces activation of RANKL-dependent Akt1 (Tu et al., 2011) in RANKL-stimulated osteoclast differentiation.

Flow cytometry analysis of osteoclasts generated from murine bone marrow cells confirmed that the adiponectin receptor AdipoR1 is expressed also by mature osteoclasts generated from murine bone marrow cells (Fig. 3d). In agreement, western-blot analysis of AMPK phosphorylation confirmed that the Adiponectin signalling pathway is active in both precursors and mature osteoclasts (Fig. 3e-g).

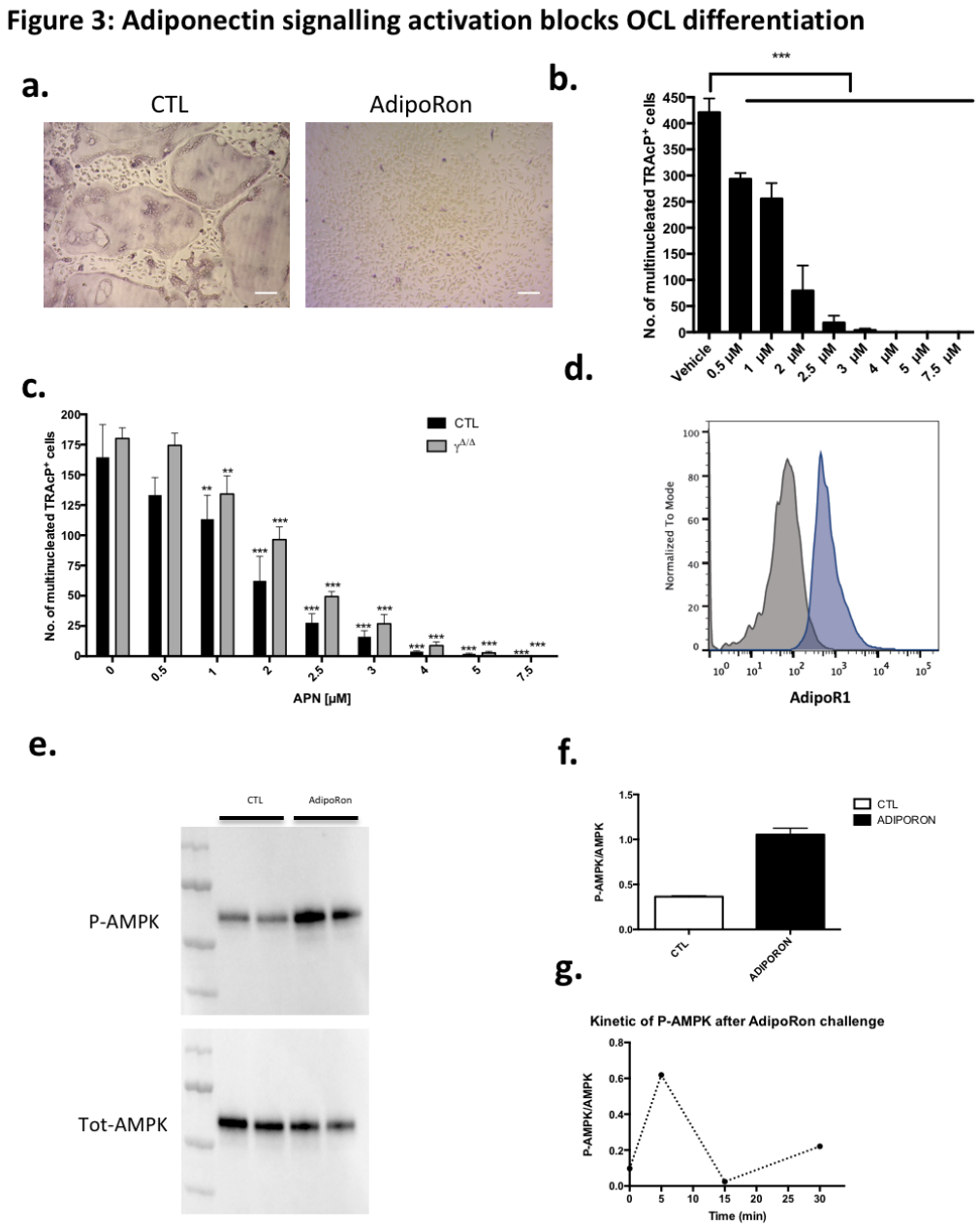

Figure 3: Adiponectin signalling activation blocks osteoclast differentiation
a. Representative images of TRAcP stained BM-derived osteoclasts differentiated in the presence or absence of AdipoRon (5µM). Scale bars=100µm. **b.** Dose response effect of AdipoRon on osteoclast differentiation using RAW264.7 cells (n=3). **c**. Effect of AdipoRon on osteoclast differentiation assay using bone marrow cells from *Pparg*$^{\Delta/\Delta}$ ($\gamma^{\Delta/\Delta}$) mice and control littermates (CTL). **d**. Expression of Type 1 Adiponectin Receptor (AdipoR1) at the surface of bone marrow derived osteoclasts demonstrated by flow cytometry. Grey curve represents unstained negative control; blue curve represents BM-derived osteoclasts. **e.** Western-blot analysis of bone marrow-derived osteoclasts treated with AdipoRon (5µM). AdipoRon treatment activates AMPK phosphorylation (p-AMPK) in murine BM-derived osteoclasts (n=2 CTL; n=2 AdipoRon stimulated) **f**. Ratio of P-AMPK over total AMPK measured by densitometry **g**. Kinetic of AMPK phosphorylation (P-AMPK) after AdipoRon challenge in RAW264.7-derived osteoclasts. Data are presented as mean ± S.E.M. Statistical significance was determined by two-tailed unpaired *t*-test.

Therefore, we investigated the consequences of adiponectin and AMPK activation on mature osteoclasts. We found that AdipoRon and AICAR, a synthetic activator of AMPK, inhibited the formation of podosomes that are essential for bone resorption (Fig. 4a,b). In addition, dorsomorphin, a reversible AMP-kinase inhibitor, could reverse the AdipoRon inhibitory effect (Fig. 4b). This is in line with the recently published effect of recombinant adiponectin on RAW264.7 cells, confirming the impact of adiponectin on both OCL differentiation and podosome formation (Chen et al., 2018) and endorsing the use of AdipoRon as a surrogate activator for Adiponectin receptors. AdipoR signalling regulates numerous cellular metabolic pathways including mitochondrial biogenesis. AdipoRon treatment provoked disruption of the perinuclear mitochondrial network in mature OCLs (Fig. 4c). Altogether, these results indicate that, beside its described inhibiting action in OCL differentiation, adiponectin signaling exerts a pivotal role in OCL energy homeostasis regulation in mature OCLs .

We next assessed the inhibitory effect of AdipoRon *in vivo* on the well-described model of osteoclast bone resorption induced by lipopolysaccharide (LPS) injection into the mouse calvaria (Fig. 4d). Both micro-CT (Fig. 4d) and TRAcP staining (Fig. 4e) showed that AdipoRon administration resulted in a strong decrease in osteoclast numbers and bone resorption pits on calvaria.

Figure 4: Adiponectin signalling regulates OCL podosome formation and activity

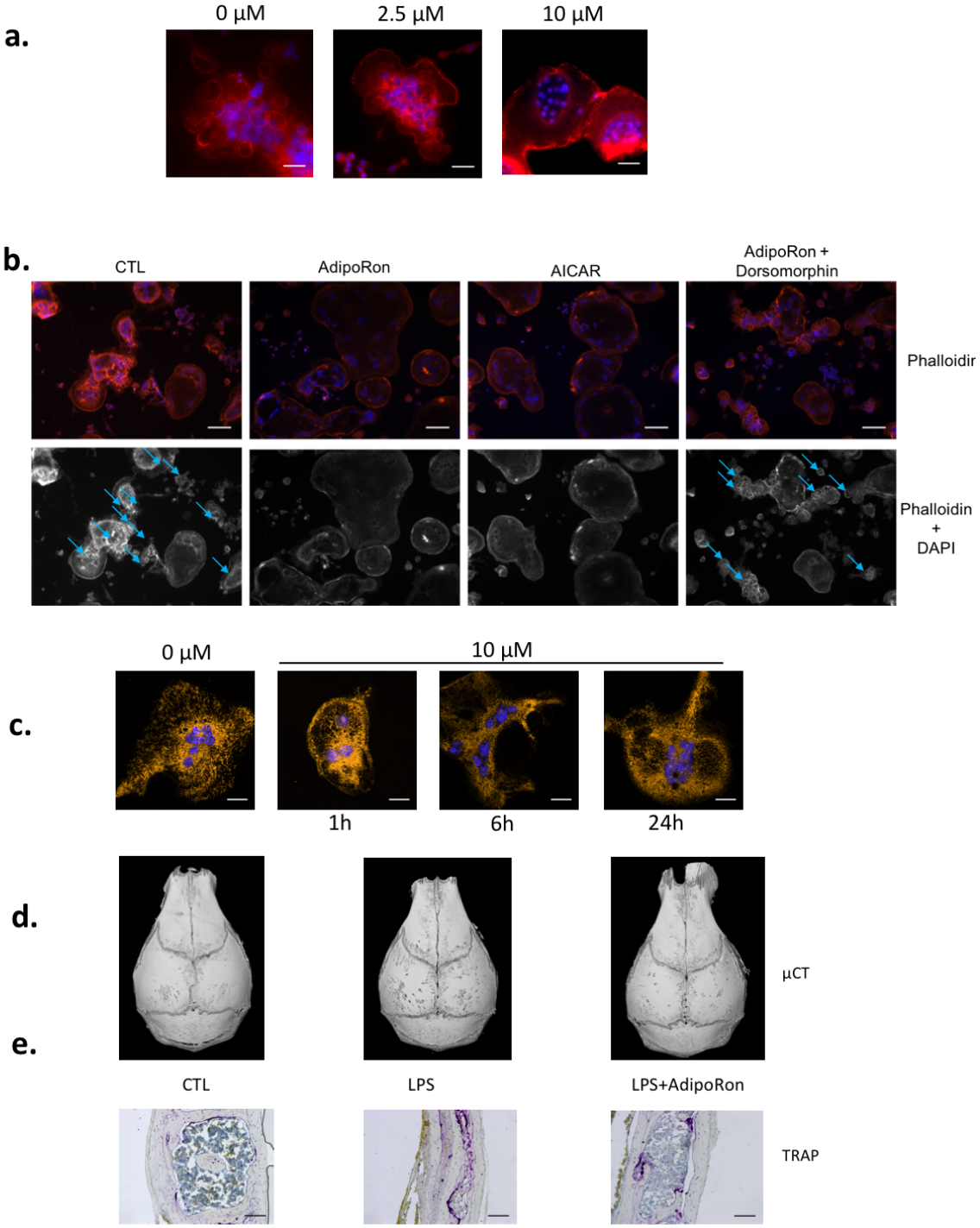

Figure 4: Adiponectin regulates OCL activity and podosome formation
a. Confocal microscopy of phalloidin-marked podosomes in RAW264.7-OCL in the presence of increasing concentrations of AdipoRon (representative images of n=3 per concentration) Scale bars=100 µm. **b.** Confocal microscopy of phalloidin-marked podosomes in the presence of AMPK modulating drugs (AdipoRon, 10µM; AICAR, 50nM; Dorsomorphin, 1.2µM)

(representative image of n=3 per conditions white asterisks mark podosomes). Scale bars=50 µm. Blue arrow indicate podosome rings. **c**. Confocal microscopy of MitoTracker Orange in mature RAW264.7-OCL after AdipoRon (10µM) challenge for different time points. Scale bars=20 µm. **d**. Micro-CT of mouse skulls collected 3 days after mice received daily *s.c.* injections on the calvaria. Mice were injected with either 100 µg lipopolysaccharide from *Salmonella abortus equi* (LPS), or 100 µg LPS + 500 ng AdipoRon (LPS + AdipoRon) or vehicle (PBS) injection (control, CTL). (n=3 animals per group) **e**.TRAcP staining of mouse skull after LPS +/- AdipoRon challenge, (representative sections, n=3 animals per group). Scale bars=100 µm.

We thus aimed to validate our findings on human cells and therefore investigated the impact of AdipoRon on hPBMC-derived OCLs. We demonstrated that low dose of AdipoRon significantly inhibits RANKL-induced OCL differentiation (Fig.S4 a and b).

We also observed that adipoRon activates AMPK phosphorylation in human PBMC-derived OCLs whithin minutes (SFig.S4 c). Finally, we showed that, within hours after the challenge with AdipoRon, the number of actin-containing podosome was drastically reduced in human OCL (SFig.4 d). These original findings offer new therapeutic perspectives in inflammatory bone loss management by targeting adiponectin/AdipoR.

Discussion

Taken together these results demonstrate that in addition to osteoblast and osteoclast precursors(Yang et al., 2019), mature osteoclasts are sensitive to extrinsic adipose-derived metabolic signals such as adipokine and that bone marrow adiposity must be considered as a physiological regulator of bone homeostasis. We show that AdipoRon, a pharmacological agonist of adiponectin receptors, inhibits osteoclast differentiation of precursors from different origins (bone-marrow, spleen and monocytic fraction). Besides its effect on osteoclast differentiation, we report here that adipoRon blocks mature osteoclast activity. Mechanistically, we demonstrate a central role for AMPK in OCL activity in this mechanism. Activation of AMPK, induced mitochondrial network alteration and podosome formation blockade, whereas AMPK blockade reverted these effects. We also demonstrate that adiponectin signaling inhibits human osteoclast differentiation but also blocks activity of human mature osteoclast. These original observations indicating a conserved adiponectin-mediated metabolic control of osteoclast activity, are clinically promising, in particular with regard to the treatment and prevention of excessive pathological bone-resorption conditions, such as in osteoporotic patients.

Metabolic sensing by osteoclasts is an emerging area of research. Whereas previous studies reported that intrinsic lipid sensing via PPARγ regulates osteoclastogenesis (Wan et al., 2007; Wei et al., 2010), we definitely demonstrate here that osteoclastogenesis can occur in the absence of PPARγ signal, and that other adipose tissue-derived signals, such as adipokine, affect osteoclast differentiation and activity. Our study paves the way for future discoveries in the dialog between adipose and bone tissue itself, both recognized as endocrine organs.

Identifiyng the source of adiponectin in the vicinity of OCL precursor and /or mature OCL in bone marrow and bone compartment is challenging. Indeed, levels of adiponectin production by BM adipocytes remains controversial since Cawthorn and coll reported that BM adipocytes serve as a major source of circulating adiponectin and exerting systemic effects during caloric restriction (Cawthorn et al., 2014) whereas others groups reported that BM adipocytes express lower levels of adiponectin than adipocytes in adipose tissue (Li et al., 2019; Liu et al., 2011; Poloni et al., 2013) .

Others sources of BM adiponectin have been recently described. BM PDGFRβ+VCAM-1+ stromal cells have been identified as major producers of adiponectin in the BM (Mukohira et al., 2019). Single cell transcriptomic profiling of the mouse bone marrow stromal compartment indicated that LepR+ BM mesenchymal stromal cells, which form a functional continuum with osteolineage cells, are expressing adiponectin (Baryawno et al., 2019). Beside their proliferative

action on HSC and antiproliferative effects on myelomonocytic and early B lymphoid cells, these adiponectin-producing cells appears to be essential to the hematopoietic niche. In this context, our finding that adiponectin regulates osteoclast activity and differentiation in bone further strengthens the argument that a metabolic pathway driven by adiponectin controls many osteoimmunology processes, including remodeling of bone marrow hematopoietic stem cell niche, with potential implications for multiple human disease states including cancer.

Finally, the inhibitory effects of adiponectin signaling on osteoclast activity and differentiation appear to be promising from a therapeutic outlook, in particular with regard to the treatment and prevention of excessive pathological bone-resorption conditions, such as in osteoporotic patients. The present study implies that preserving functional adiponectin sensitivity in patients suffering from metabolic diseases (e.g. diabetes, obesity, metabolic syndrome) might be also beneficial for preventing bone frailty.

Supplemental data

Figure S1

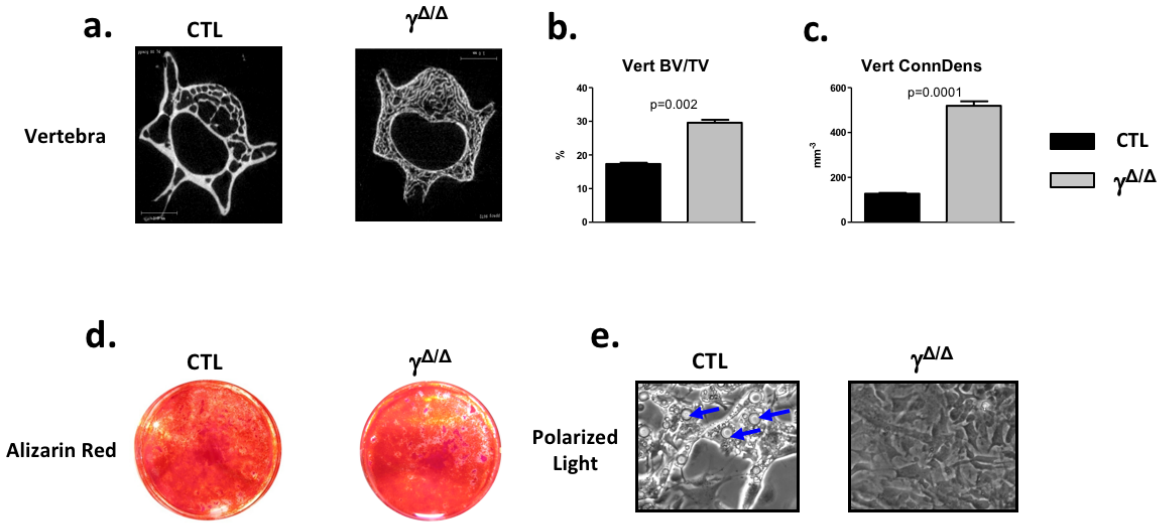

Supplemental Data Figure 1: Osteoblastic activity is increased in mice with epiblastic deletion of PPARγ. a. Representative 3-D micro-CT of the fourth lumbar vertebrae of CTL and $\gamma^{\Delta/\Delta}$ mice. n = 5 WT and 5 $\gamma^{\Delta/\Delta}$. **b.** Trabecular bone volume fraction measured by micro-CT analysis of vertebra from $\gamma^{\Delta/\Delta}$ (n=5) and control (CTL; n=5) littermates. **c.** Trabecular connectivity density measured by micro-CT analysis of vertebra from $\gamma^{\Delta/\Delta}$ (n=5) and control (CTL; n=5) littermates. **d.** Primary osteoblast differentiation and proliferation in culture of calvaria pre-osteoblast from of newborn CTL and $\gamma^{\Delta/\Delta}$ pups. Alizarin red S staining of calcium deposition was conducted in osteoblasts cultured 3 weeks after changing to osteogenic medium (containing 50 µg/ml ascorbic acid and 100 nM β-glycerolphosphate). **e.** Primary adipocyte differentiation from bone marrow mesenchymal stem cell obtained from of newborn CTL and $\gamma^{\Delta/\Delta}$ pups 3 weeks after changing to adipogenic medium (containing dexamethasone (2.5 µM), 3-isobutyl-1-methylxanthine (0.5 mM) and insulin (10 µg/mL)). Blue arrow indicates lipid droplets.

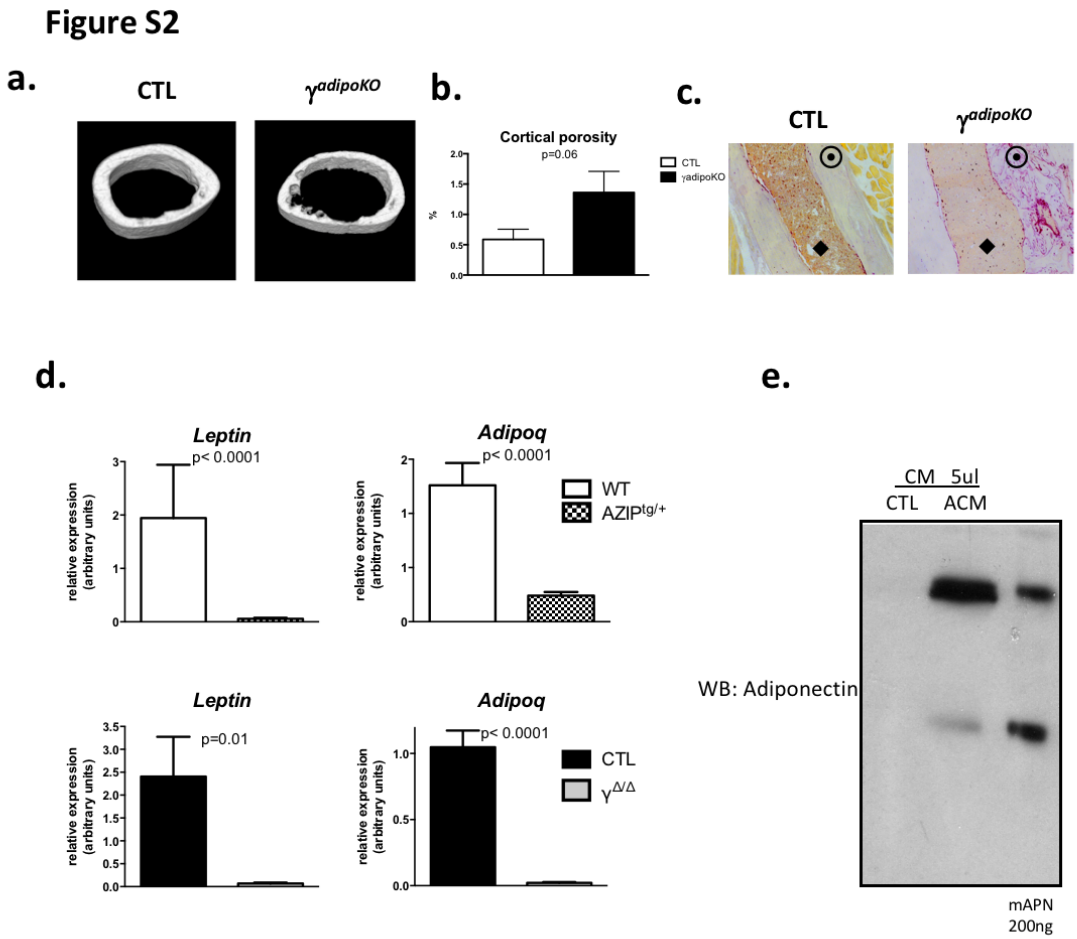

Supplemental Data Figure 2: Increased cortical porosity in a mouse model of lipoatrophy with functional PPARγ. a. Representative 3D sections of midshaft femur from $\gamma^{adipoKO}$ (n=3) and CTL (n=3) littermates. **b.** Femoral cortical porosity measured by micro-CT analysis of femur from $\gamma^{adipoKO}$ (n=3) and control (CTL; n=3) littermates. **c.** Representative images of TRAcP staining of longitudinal sections of decalcified femurs, at mid-shaft levels, from control (CTL) or $\gamma^{adipoKO}$ mice. ⊙ = cortical bone; ◆ = bone marrow. **d.** RT-qPCR analysis of *Leptin* and *AdipoQ* mRNA levels in long bone from A-ZIP$^{tg/+}$(n=8) and their CTL littermates (n=8) and from $\gamma^{\Delta/\Delta}$ (n=7) and their CTL littermates (n=6). Data are presented as mean ± S.E.M. Statistical significance was determined by two-tailed unpaired *t*-test. **e**. Western-blot analysis of conditioned medium from undiffentiated (CTL) and differentiated 3T3-L1 adipocyte (A-CM) against adiponectin. Recombinant adiponectin (200ng rmAdiponectin) was added to demonstrate specificity of the signal.

Figure S3

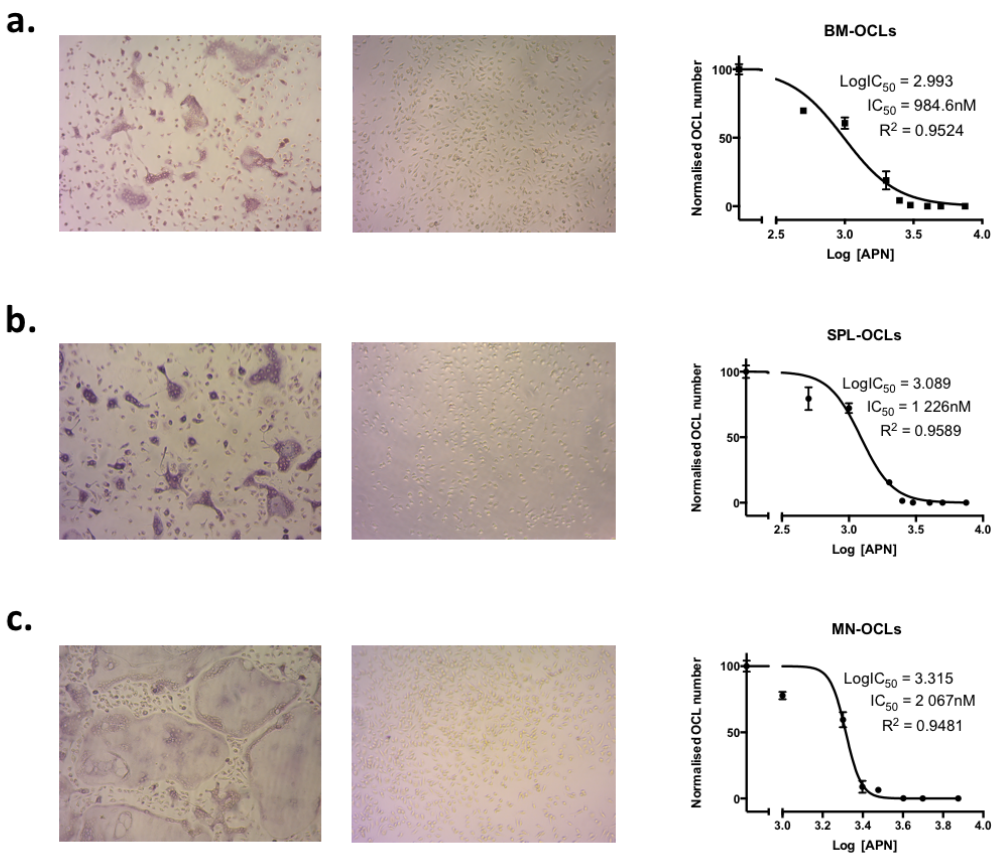

Supplemental Data Figure 3: AdipoRon inhibits OCL differentiation of multiple origins. *left panel.* Representative images of TRAcP stained (**a**.) BM-derived, (**b**.) spleen derived and (**c**.) macrophages enriched fraction osteoclasts differentiated in the presence or absence of AdipoRon (5µM). *right panel*, The mean IC50 of AdipoRon inhibition of OCL differentiation was determined from the curve with the error of the fit (S.E.M.) Data are mean ± S.E.M. (n = 3 biological replicates).

Figure S4: AdipoRon inhibits human OCL differentiation and activity

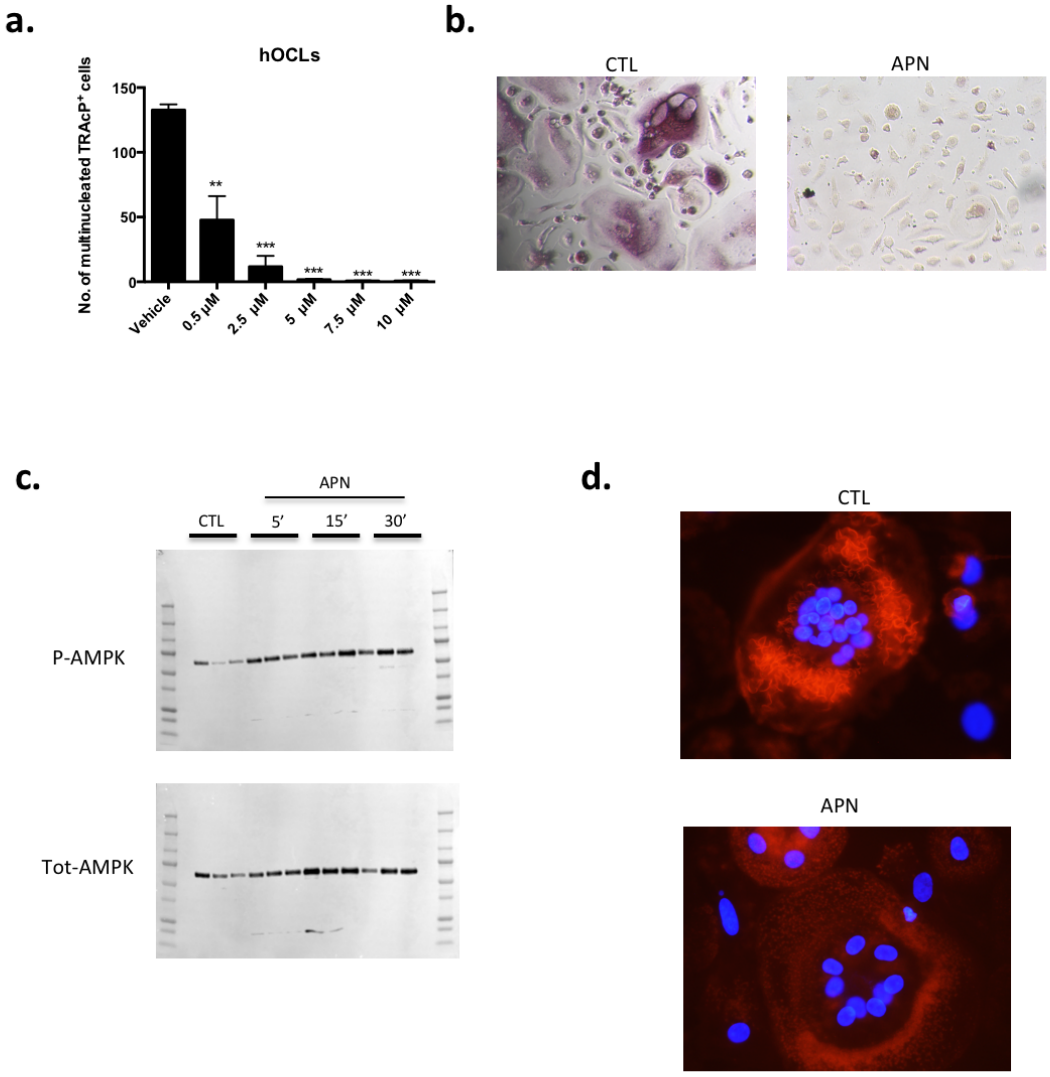

Figure S4: AdipoRon inhibits human OCL differentiation and activity through AMPK activation. a. Dose response effect of AdipoRon on osteoclast differentiation from hPBMC (n=5). **b.** Representative images of TRAcP staining of hPBMC derived osteoclast differentiation in the presence or absence of AdipoRon (5µM). **c.** Western-blot analysis of hPBMC-derived osteoclasts treated with AdipoRon (5µM). AdipoRon treatment (5', 15', 30') activates AMPK phosphorylation (p-AMPK) in hPBMC. **d.** Fluorescence microscopy of phalloidin-marked podosomes in hPBMC derived OCL in the presence of AdipoRon (5µM, 12h) (representative images of n=5).

Material & Methods

Key ressources table

REAGENT or RESOURCE	SOURCE	IDENTIFIER
Antibodies		
Neutralizing adiponectin receptor 1 polyclonal antibody	Enzo Life Science	ALX-210-645-C200
Adiponectin rabbit monoclonal antibody	Cell Signaling Technology	#2789
AMPKα Rabbit mAb (D63G4)	Cell Signaling Technology	#5832
Phospho-AMPKα (Thr172) (40H9) Rabbit mAb	Cell Signaling Technology	#2535
Chemicals, Peptides, and Recombinant Proteins		
Fetal Bovine Serum	GIBCO	10082139
Alpha MEM with NTP, dNTP	GIBCO	22571
AdipoRon	SIGMA	SML0998
mRANKL	R&D systems	462-TEC
hRANKL	R&D systems	6449-TEC
Critical Commercial Assays		
Acid Phosphatase, Leukocyte (TRAP) assay	SIGMA	387A
murine serum CTX ELISA	LSBio	F21349
murine serum OCN ELISA	LSBio	F12227
murine serum PTH ELISA	LSBio	F23085
Experimental Models: Cell Lines		
3T3-L1 pre adipose murine cell line	ATCC	CL-173
RAW 264.7 murine macrophage	ATCC	TIB-71
Experimental Models: Organisms/Strains		
Sox2-Cre mouse	The Jackson Laboratory	004783
Adipoq-Cre mouse	The Jackson Laboratory	010803
PPARg L2/L2 mouse	B Desvergne	PMID:15070754
AZIP/F1 tg mouse	C Vinson	PMID:9784492
Oligonucleotides		
Gapdh		Sup Table1
ActB		Sup Table1
AdipoQ		Sup Table1
Leptin		Sup Table1
Software and Algorithms		
CTan CTVol	Skyscan	
ImageJ	Fiji	

Mouse models

Genotype denomination follows, the rules recommended by the Mouse Genome Database (MGD) Nomenclature Committee. Animal procedures were authorized by the Canton of Vaud veterinary service. Sox2CRE transgenic mice (SOX2CRE$^{tg/+}$; Tg(Sox2-cre)1Amc/J) and AdipoQCRE (*Adipoq-Cre*$^{tg/+}$) from The Jackson Laboratory, were maintained in the University of Lausanne Animal Facility. The series of matings allowing the generation of the

SOX2CRE$^{tg/+}$*Pparg*$^{em\Delta/\Delta}$ mouse (hereafter called *Pparg*$^{\Delta/\Delta}$), which expressed the SOX2CRE transgene and have no *Pparg* functional alleles, as well as their control littermates (CTL) that have no SOX2CRE transgene and two functional *Pparg* alleles (*Pparg*$^{fl/+}$) have been described in (Gilardi et al., 2019). γ^{FatKO} and their control littermates were generated as described in (Wang et al., 2013a). AZIP/F1 mice on FVB background (Tg(AZIP/F)1Vsn in MGD, hereafter called AZIP$^{tg/+}$) and wild type FVB controls were a kind gift from Dr. Charles Vinson and were generated as previously described (Moitra et al., 1998).

Primary cell culture

Bone marrow (BM) cells were isolated by crushing entire long bones into DMEM/3% FCS (GIBCO). Bone fragments were removed by filtration through a 70 µm filter mesh. Splenocyte suspensions were obtained by mashing the spleen through sieves into DMEM/3% FCS, washing by centrifugation then filtering through 70 µm filter caps. Primary osteoblasts from neonatal calvaria of *Pparg*$^{fl/+}$ and *Pparg*$^{\Delta/\Delta}$ were harvested by sequential collagenase type II (3 mg/mL) digestions of individual calvarium from 2 to 3-day-old mice. After genotyping, calvaria cells of the same genotype were pooled and plated accordingly. The cells were incubated at 37° C with 5% CO2 and media was changed every two days until they reached 80% confluency. To assess proliferation, primary osteoblasts were plated in 24-well plates at a concentration of 10,000 cells/well in EMEM media (GIBCO) containing 10% FBS, 100 U/ml penicillin and 100 ug/ml streptomycin (GIBCO).

Osteoclastogenesis Assays and TRAcP staining of murine and human primary cells

Erythrocytes were eliminated from murine splenocyte and BM preparation or human PBMC using ACK lysis buffer. Cells were cultured in complete αMEM with 40 ng/ml M-CSF (ProSpec-Tany TechnoGene, Rehovat, Israel) and l0 ng/ml RANKL (R&D Systems, MN). Tartrate-resistant acid phosphatase (TRAcP) staining was performed after 4-6 days, using the Acid Phosphatase, Leukocyte (TRAP) Kit according to the manufacturer's instructions (Sigma). Mature osteoclasts were identified as multi-nucleate TRAcP^{+} cells using light microscopy. 3T3-L1 cells (ATCC) were grown to sub-confluence in DMEM/10% FBS. Cells were then cultured in adipogenic conditions (DMEM/10%FBS, 0.5 mM 3-isobutyl-1-methylxanthine, 1 µM dexamethasone (Sigma), and 10 µg/ml bovine insulin (Sigma)) for 2 weeks, after which the medium was changed back to DMEM/10% FBS. Adipocyte Conditioned Medium (A-CM) was collected after 24 hours exposure to differentiated cells. Similarly, conditioned control medium (CTL) was obtained from undifferentiated 3T3-L1 cells. A-CM

and CTL were concentrated 5X using Centriprep™ (Millipore). Conditioned medium from either differentiated or undifferentiated 3T3-L1 cells was added during osteoclastogenesis from multipotent progenitor cells. For neutralisation experiments, 50% CM was incubated with different amounts of anti-adiponectin antibody (Enzo Life Sciences) for 30 min at room temperature then added during osteoclastogenesis. TRAcP staining to evaluate osteoclast numbers was performed as mentioned above.

Osteoclast differentiation and TRAcP staining of RAW 264.7 cells

For osteoclastogenesis, a total of $1x10^4$ RAW 264.7 (ATCC) cells were seeded per well on 24-well plates in 500 µl αMEM containing 5% FCS (Hyclone, GE Healthcare), 1% penicillin-streptomycin (Gibco) as well as 50 µM β-mercaptoethanol (Gibco) and 30 ng/ml murine RANKL (R&D Systems). To study the impact of adiporon on osteoclast differentiation, 10 µM AdipoRon (Sigma-Aldrich) were added to the culture medium. Tartrate-resistant acid phosphatase (TRAcP) activity was examined using the leucocyte acid phosphatase kit (Sigma-Aldrich) according to manufacturer's specifications. $TRAcP^+$ cells with ≥3 nuclei were considered as osteoclasts. In addition, $5x10^3$ RAW 264.7 cells were seeded per well in a Nunc Lab-Tek II 8-well Chamber Slide system (ThermoFisher Scientific) in a total of 300 µl osteoclast differentiation medium containing 30 ng/ml RANKL. Fully differentiated osteoclasts were treated with 10 µM AdipoRon for the indicated time points. FACS analysis as well as sorting of mature OCLs for subsequent Western-blot analyses was performed as described previously(Madel et al., 2018).

Measurement of bone morphology and microarchitecture

Bone mineral density (BMD mg/cm^2) and bone mineral content (BMC mg) of femurs were measured *ex vivo* using dual energy X-ray absorptiometry (pDXA; PIXImus, GE- Lunar Corp.). High-resolution micro-computed tomography (UCT40, ScancoMedical AG, Bassdorf, Switzerland) was used to scan the femur and the 5th lumber vertebral body. Cortical and trabecular bones were evaluated using isotropic 12µm voxels. For trabecular bones, we assessed bone volume fraction (BV/TV, %), trabecular thickness (Tb.Th, µm), trabecular number (Tb.N, mm^{-1}), and trabecular separation (Tb.Sp, µm). For cortical midshaft femur, we measured the average total volume (TV, mm^3), bone volume (BV, mm^3) and average cortical thickness (µm). SkyScan software (CTAn and CTVol) was employed to calculate cortical bone porosity of femur using a dedicate method after acquisition using a Skyscan 1272 (SkyScan 1272, Bruker, Brussels, Belgium) at a resolution of 10 µm/pix and visualized in 3D.

Serum protein assays

Blood was obtained by cardiac puncture immediately after euthanasia. After clotting and centrifugation, serum was collected and stored at -80°C until use. Serum CTX (carboxy-terminal collagen crosslinks), osteocalcin (OCN), alkaline phosphatase (ALP) and parathyroid hormone (PTH) were measured by ELISA assays according to the manufacturer's protocol (LifeSpan Biosciences, Inc., Seattle, WA).

Calvaria injection

Nine 6-week old C57/BL6 male mice were purchased from Envigo and housed in the local animal facility under a 12h light/12h dark cycle. The animals were randomly divided into three experimental groups, each group comprising three mice. Mice received daily *s.c.* injections on the calvaria before analysis on the third day. Group 1 was injected with 100 µg lipopolysaccharide from *Salmonella abortus equi* (LPS, Sigma-Aldrich), group 2 with 100 µg LPS + 500 ng AdipoRon (Sigma-Aldrich) and experimental group 3 underwent vehicle (PBS) injection. Calvariae were collected and fixed overnight in 4% formaldehyde at 4°C and then stored in 70% EtOH. Subsequent micro-CT analysis were used to evaluate the resorbed area. Calvariae were decalcified in 10% EDTA, embedded in paraffin and 5-micron sections were cut and stained for tartrate-resistant acid phosphatase (TRAcP, Sigma-Aldrich).

Quantitative RT-PCR

Total RNA was isolated from total long bones, including the crude BM, or primary cell cultures, using TRIzol LS (Invitrogen) and purified with the RNeasy kit (Qiagen). RNA quality was verified by microfluidic (Agilent 2100 Bioanalyzer) and concentration determined with a NanoDrop spectrophotometer (Wilmington). Total RNA (500 ng/µg) was reverse transcribed using Script^{TM} cDNA synthesis kit (Bio-Rad) according to the manufacturer's instructions. Real time qPCR was performed with SYBR® Green PCR mastermix using an ABI PRISM® 7900 PCR machine (Applied Biosystems). Results were normalized to glyceraldehyde-3-phosphate dehydrogenase (*Gapdh*) or beta-actin beta (*Actb*).

Western blot anlysis

Sorted mature OCLs were washed twice with ice-cold PBS and scraped in 1X Laemmli buffer. Cells were disrupted by sonication and centrifuged at 3000 rpm for 10 min. Protein samples were analyzed by SDS/PAGE (gradient 4-15% acrylamide, Criterion, BioRad) and electroblotted onto 0.2% PVDF membrane using Transblot Turbo (BioRad). After 1 h in

blocking buffer (Tris-buffered saline (TBS)–Tween 20 with 5% fat free dry milk), membranes were blotted overnight at 4°C with Rabbit mAb against AMPKα (D63G4) (dilution 1:1 000, Cell Signaling Technology) or Phospho-AMPKα (Thr172) (40H9) (dilution 1 :1000, Cell Signaling Technology), diluted in TBS–Tween with 5% BSA. After three washing steps with TBS–Tween 20, blot was incubated for 1 h at room temperature with anti-rabbit IgG conjugated with horseradish peroxidase diluted 1:2000 in blocking buffer. After four additional washing steps with TBS–Tween 20, protein bands were detected by chemiluminescence using Chemi Doc XRS+ (BioRad).

Imaging

Podosomes were visualized by phalloidin staining (Sigma-Aldrich) following manufacturer's instructions. After removing unbound phalloidin conjugates, cells were labelled with 1 µg/ml DAPI (Sigma-Aldrich). Microscopic imaging was performed using a fluorescence microscope (Zeiss Axio Observer D1). For mitochondrial analysis, live cells were labeled with 200 nM MitoTracker Orange (ThermoFisher) according to manufacturer's recommendations. After staining, cells were fixed in 4% formaldehyde, labelled with 1 µg/ml DAPI and subjected to z-stack confocal microscopy analyses (Zeiss LSM 710 on an inverted Axio Observer.Z1 stand). Images were processed using Fiji/Image J software(Schindelin et al., 2012).

Statistical analysis

The data were analyzed using one- or two-factor ANOVA for multiple comparisons as appropriate. Two-group comparisons were performed using the Student's *t*-test. ns: non-significant, * $p<0.05$, ** $p<0.01$, *** $p< 0.001$, **** $p<0.0001$.

Acknowledgements

This work was supported by the Etat de Vaud (BD and AW) the FNRS (BD), the Région Grand Est (J-YJ), the Fondation Arthritis (DM) and by the french PIA project Lorraine Université d'Excellence, reference ANR-15-IDEX-04-LUE (J-YJ and DM).

Authors contribution

HF designed the experimental plan, performed the experiments, analyzed the data, and contribute to the original draft preparation. MBM, DDP, MS, CW, AW, CP, and BT performed experiments, analyzed the data, and prepared the vizualisation. JYJ, FG, SF, NB and CBW contributed to the conceptualization, analyzed the data, and reviewed/edited the manuscript. BD and DM conceived the study, designed the experimental plan, supervised the study, analyzed the data, wrote the manuscript, and acquired financial support for the project. All authors read and edited the manuscript. BD and DM are the guarantors of this work and, as such, had full access to all the data in the study and take responsibility for the integrity of the data and the accuracy of the data analyses.

References

Akune, T., Ohba, S., Kamekura, S., Yamaguchi, M., Chung, U.-I., Kubota, N., Terauchi, Y., Harada, Y., Azuma, Y., Nakamura, K., Kadowaki, T., Kawaguchi, H., 2004. PPARgamma insufficiency enhances osteogenesis through osteoblast formation from bone marrow progenitors. J. Clin. Invest. 113, 846–855. doi:10.1172/JCI19900

Barak, Y., Nelson, M.C., Ong, E.S., Jones, Y.Z., Ruiz-Lozano, P., Chien, K.R., Koder, A., Evans, R.M., 1999. PPAR gamma is required for placental, cardiac, and adipose tissue development. Mol. Cell 4, 585–595.

Baryawno, N., Przybylski, D., Kowalczyk, M.S., Kfoury, Y., Severe, N., Gustafsson, K., Kokkaliaris, K.D., Mercier, F., Tabaka, M., Hofree, M., Dionne, D., Papazian, A., Lee, D., Ashenberg, O., Subramanian, A., Vaishnav, E.D., Rozenblatt-Rosen, O., Regev, A., Scadden, D.T., 2019. A Cellular Taxonomy of the Bone Marrow Stroma in Homeostasis and Leukemia. Cell 177, 1915–1932.e16. doi:10.1016/j.cell.2019.04.040

Cawthorn, W.P., Scheller, E.L., Learman, B.S., Parlee, S.D., Simon, B.R., Mori, H., Ning, X., Bree, A.J., Schell, B., Broome, D.T., Soliman, S.S., DelProposto, J.L., Lumeng, C.N., Mitra, A., Pandit, S.V., Gallagher, K.A., Miller, J.D., Krishnan, V., Hui, S.K., Bredella, M.A., Fazeli, P.K., Klibanski, A., Horowitz, M.C., Rosen, C.J., MacDougald, O.A., 2014. Bone Marrow Adipose Tissue Is an Endocrine Organ that Contributes to Increased Circulating Adiponectin during Caloric Restriction. Cell Metab. 20, 368–375. doi:10.1016/j.cmet.2014.06.003

Chen, G., Huang, L., Wu, X., Liu, X., Xu, Q., Li, F., Dai, M., Zhang, B., 2018. Adiponectin inhibits osteoclastogenesis by suppressing NF-κB and p38 signaling pathways. Biochem. Biophys. Res. Commun. 503, 2075–2082. doi:10.1016/j.bbrc.2018.07.162

Gilardi, F., Winkler, C., Quignodon, L., Diserens, J.-G., Toffoli, B., Schiffrin, M., Sardella, C., Preitner, F., Desvergne, B., 2019. Systemic PPARγ deletion in mice provokes lipoatrophy, organomegaly, severe type 2 diabetes and metabolic inflexibility. Metab. Clin. Exp. doi:10.1016/j.metabol.2019.03.003

Horowitz, M.C., Berry, R., Holtrup, B., Sebo, Z., Nelson, T., Fretz, J.A., Lindskog, D., Kaplan, J.L., Ables, G., Rodeheffer, M.S., Rosen, C.J., 2017. Bone marrow adipocytes. Adipocyte 6, 193–204. doi:10.1080/21623945.2017.1367881

Imai, T., Takakuwa, R., Marchand, S., Dentz, E., Bornert, J.-M., Messaddeq, N., Wendling, O., Mark, M., Desvergne, B., Wahli, W., Chambon, P., Metzger, D., 2004. Peroxisome proliferator-activated receptor gamma is required in mature white and brown adipocytes for their survival in the mouse. Proceedings of the National Academy of Sciences 101, 4543–4547. doi:10.1073/pnas.0400356101

Iwaki, M., Matsuda, M., Maeda, N., Funahashi, T., Matsuzawa, Y., Makishima, M., Shimomura, I., 2003. Induction of adiponectin, a fat-derived antidiabetic and antiatherogenic factor, by nuclear receptors. Diabetes 52, 1655–1663.

Li, Y., Meng, Y., Yu, X., 2019. The Unique Metabolic Characteristics of Bone Marrow Adipose Tissue. Front Endocrinol (Lausanne) 10, 69. doi:10.3389/fendo.2019.00069

Liu, L.-F., Shen, W.-J., Ueno, M., Patel, S., Kraemer, F.B., 2011. Characterization of age-related gene expression profiling in bone marrow and epididymal adipocytes. BMC Genomics 12, 212. doi:10.1186/1471-2164-12-212

Madel, M.-B., Ibáñez, L., Rouleau, M., Wakkach, A., Blin-Wakkach, C., 2018. A Novel Reliable and Efficient Procedure for Purification of Mature Osteoclasts Allowing Functional Assays in Mouse Cells. Front Immunol 9, 2567. doi:10.3389/fimmu.2018.02567

Moitra, J., Mason, M.M., Olive, M., Krylov, D., Gavrilova, O., Marcus-Samuels, B., Feigenbaum, L., Lee, E., Aoyama, T., Eckhaus, M., Reitman, M.L., Vinson, C., 1998. Life without white fat: a transgenic mouse. Genes Dev. 12, 3168–3181.

Mukohira, H., Hara, T., Abe, S., Tani-ichi, S., Sehara-Fujisawa, A., Nagasawa, T., Tobe, K., Ikuta, K., 2019. Mesenchymal stromal cells in bone marrow express adiponectin and are efficiently targeted by an adiponectin promoter-driven Cre transgene. Int. Immunol. 45, 1219–13. doi:10.1093/intimm/dxz042

Okada-Iwabu, M., Yamauchi, T., Iwabu, M., Honma, T., Hamagami, K.-I., Matsuda, K., Yamaguchi, M., Tanabe, H., Kimura-Someya, T., Shirouzu, M., Ogata, H., Tokuyama, K., Ueki, K., Nagano, T., Tanaka, A., Yokoyama, S., Kadowaki, T., 2013. A small-molecule AdipoR agonist for type 2 diabetes and short life in obesity. Nature 503, 493–499. doi:10.1038/nature12656

Oshima, K., Nampei, A., Matsuda, M., Iwaki, M., Fukuhara, A., Hashimoto, J., Yoshikawa, H., Shimomura, I., 2005. Adiponectin increases bone mass by suppressing osteoclast and activating osteoblast. Biochem. Biophys. Res. Commun. 331, 520–526. doi:10.1016/j.bbrc.2005.03.210

Poloni, A., Maurizi, G., Serrani, F., Mancini, S., Zingaretti, M.C., Frontini, A., Cinti, S., Olivieri, A., Leoni, P., 2013. Molecular and functional characterization of human bone marrow adipocytes. Exp. Hematol. 41, 558–566.e2. doi:10.1016/j.exphem.2013.02.005

Rosen, E.D., Sarraf, P., Troy, A.E., Bradwin, G., Moore, K., Milstone, D.S., Spiegelman, B.M., Mortensen, R.M., 1999. PPAR gamma is required for the differentiation of adipose tissue in vivo and in vitro. Mol. Cell 4, 611–617.

Schindelin, J., Arganda-Carreras, I., Frise, E., Kaynig, V., Longair, M., Pietzsch, T., Preibisch, S., Rueden, C., Saalfeld, S., Schmid, B., Tinevez, J.-Y., White, D.J., Hartenstein, V., Eliceiri, K., Tomancak, P., Cardona, A., 2012. Fiji: an open-source platform for biological-image analysis. Nat. Methods 9, 676–682. doi:10.1038/nmeth.2019

Takada, I., Kouzmenko, A.P., Kato, S., 2009. Wnt and PPARγ signaling in osteoblastogenesis and adipogenesis. Nature Reviews Rheumatology 5, 442–447. doi:10.1038/nrrheum.2009.137

Tontonoz, P., Spiegelman, B.M., 2008. Fat and beyond: the diverse biology of PPARgamma. Annu. Rev. Biochem. 77, 289–312. doi:10.1146/annurev.biochem.77.061307.091829

Tu, Q., Zhang, J., Dong, L.Q., Saunders, E., Luo, E., Tang, J., Chen, J., 2011. Adiponectin inhibits osteoclastogenesis and bone resorption via APPL1-mediated suppression of Akt1. J. Biol. Chem. 286, 12542–12553. doi:10.1074/jbc.M110.152405

Wan, Y., Chong, L.-W., Evans, R.M., 2007. PPAR-γ regulates osteoclastogenesis in mice. Nat Med 13, 1496–1503. doi:10.1038/nm1672

Wang, F., Mullican, S.E., DiSpirito, J.R., Peed, L.C., Lazar, M.A., 2013a. Lipoatrophy and severe metabolic disturbance in mice with fat-specific deletion of PPAR. Proceedings of the National Academy of Sciences 110, 18656–18661. doi:10.1073/pnas.1314863110

Wei, W., Wang, X., Yang, M., Smith, L.C., Dechow, P.C., Sonoda, J., Evans, R.M., Wan, Y., 2010. PGC1beta mediates PPARgamma activation of osteoclastogenesis and rosiglitazone-induced bone loss. Cell Metab. 11, 503–516. doi:10.1016/j.cmet.2010.04.015

Yamaguchi, N., Kukita, T., Li, Y.-J., Kamio, N., Fukumoto, S., Nonaka, K., Ninomiya, Y., Hanazawa, S., Yamashita, Y., 2008. Adiponectin inhibits induction of TNF-alpha/RANKL-stimulated NFATc1 via the AMPK signaling. FEBS Lett. 582, 451–456. doi:10.1016/j.febslet.2007.12.037

Yang, J., Park, O.-J., Kim, J., Han, S., Yang, Y., Yun, C.-H., Han, S.H., 2019. Adiponectin Deficiency Triggers Bone Loss by Up-Regulation of Osteoclastogenesis and Down-

Regulation of Osteoblastogenesis. Front Endocrinol (Lausanne) 10, 815. doi:10.3389/fendo.2019.00815
Zou, W., Rohatgi, N., Chen, T.H.-P., Schilling, J., Abu-amer, Y., Teitelbaum, S.L., 2016. PPAR-γ regulates pharmacological but not physiological or pathological osteoclast formation. Nat Med 22, 1203–1205. doi:10.1038/nm.4208